ICGEB International Centre for Genetic Engineering and Biotechnology | Developing Knowledge

ICGEB Research Grants Programme

RESEARCH GRANTS COMPLETED in 2021

CRP - ICGEB RESEARCH GRANTS COMPLETED IN 2021

COUNTRY	PRINCIPAL INVESTIGATOR	PROJECT TITLE
BANGLADESH	Haseena KHAN	Elucidation of taxol biosynthetic pathway in entophytic fungi *Grammothele lineata* - SDL-CO-2015-S1
COLOMBIA	Maria Teresa RUGELES LOPEZ	Phenotypic and functional characterization of the adaptive immune response during differential progression of COVID-19 (*funded by IILA*)
KENYA	Steven RUNO	Deciphering resistance and virulence in sorghum-*Striga* interaction
KENYA	Tindih Sheltone HESHBORNE	Characterization of the SARS-CoV-2 virus and antibodies
MALAYSIA	Reena RAJASURIAR	D-amino acids as potential modulators of age-related functional decline in natural and accelerated aging
MALAYSIA	Ling Ling TAN	Nanomaterials based-Genosensor (Nano-GS) for improved detection method of SARS-CoV-2 RNA as rapid COVID-19 diagnosis strategy
PAKISTAN	Aamir SHEHZAD *Former PI: Moazur Rahman*	Development of recombinant vaccine to combat inclusion-body hepatitis-hydropericardium syndrome in poultry
RUSSIA	Sergey A. KOZIN	Role of zinc-driven interaction of amyloid-beta with neuronal proteins in Alzheimer's disease
TURKEY	Ayse KOCA CAYDASI	Functional and molecular characterization of novel mitotic exit inhibitors *(Early Career Return Grant*)
VIET NAM	Hanh Hong MAI	Development a simple, low-cost, high sensitivity fluorescent biosensor for hydrogen peroxide (H_2O_2), glucose and cholesterol sensing based on ZnO nanorods decorated metal nanoparticles

BANGLADESH

Title: Elucidation of taxol biosynthetic pathway in endophytic fungus *Grammothele lineata* -SDLCO-2015-S1

Principal Investigator: Haseena Khan, Molecular Biology Laboratory, Department of Biochemistry and Molecular Biology, Faculty of Biological Sciences, University of Dhaka, Dhaka 1000, Bangladesh. Tel: +880-1711612344, Fax: +880-2-9667222, Email haseena@du.ac.bd

ICGEB Contract No.: CRP/ BGD17-01

ICGEB Reference No.: CRP/17/003

Abstract: Initial screening had confirmed the production of taxol by *Grammothele lineata* -SDLCO-2015-S1, an endofungus isolated from jute. Subsequent investigation for taxol production could not be reproduced and biosynthetic pathway could not be elucidated. While searching for taxol the strain was found to harbor biosynthetic gene cluster for another anticancer drug, epothilone. Both the genome and RNA-Seq data showed the presence of epothilone gene clusters in *G. lineata*. TLC, LC-MS/MS were used to isolate and characterise epothilone. Purified sample showed signal at ($M+H^+$) = 508.1 Da, identical to standard epothilone B. Product ions were found with the m/z values at 321.2 Da, 421.2 Da; atypical MS2 fragments for standard Epothilone B. Investigation of *G. lineata* genome using bioinformatic tools for industrially important enzymes and secondary metabolites allowed identification of 28 gene clusters for secondary metabolites and a diverse range of CAZymes, including numerous lignocellulolytic enzymes. Transcriptome and secretome analyses of *G. lineata* were performed to understand the lignocellulosic enzyme production capacity, nature of the enzymes, and their possible use for biomass hydrolysis. A study of untargeted metabolomics led to the identification of artemisinin, a widely known antimalarial compound.

Objectives:

(i) *In silico* prediction of Taxol biosynthetic pathway in *Grammothele lineata* through genome analysis. (Initially this was not enumerated as an objective of the proposal. However, since the genome sequence was available it was thought pertinent to try and elucidate the taxol biosynthetic pathway in the endofungus as this would be highly relevant to the project);
(ii) Optimisation of the growth conditions and other parameters for taxol production and quantification;
(iii) Identification of the optimum combination of elicitors (media optimisation). List of reported elicitors expected to increase taxol production includes methyl jasmonate (MJ), vanadyl sulfate (VS), salicylic acid (SA), phenylalanine, benzoic acid, indole acetic acid (IAA) and cobalt chloride;
(iv) Quantification of the amount of taxol produced for each combination of elicitors after 15 to 21 days;
(v) Isolation of total RNA from control and optimised elicitors at 4 different time intervals starting from 15 to 21 days;
(vi) RNA -sequencing analysis using Illumina Hi-seq platform;
(vii) Isolation of total protein from control media and optimised elicitor media at 4 different time intervals;
(viii) Proteomics analysis using LC-ESI-MS/MS iTRAQ labeling;
(ix) Annotation of proteo-transcriptomics data and identification of the overlapping elicited pathway.

Results Obtained:

G. lineata is under the Basidiomycota phylum and fungi under the phylum of Basidiomycota are known to produce a variety of cytotoxic compounds (Rosa et al., 2009). Thus, *G. lineata* with the ability to produce epothilone was not found to be surprising. The epothilones are a class of potential cancer drugs. Like taxanes, they prevent cancer cells from dividing by interfering with tubulin, but in early trials epothilones have been shown to have better efficacy and milder adverse effects than taxanes. BLASTx has also been carried out for the RNA-Seq data generated in this project primarily for identifying taxol biosynthetic pathway. For identifying the epothilone gene cluster the *G. lineata* transcripts were matched for homology with epothilone gene clusters identified from the genome analysis. Each of these clusters showed 100% similarity with two of the genes from the RNA-Seq data. In order to establish epothilone production capacity of the fungus, purification of the compound was carried out using thin layer chromatography along with standard Epothilone B. Later, MS-MS identified the molecular weight of epothilone B. Mass-spectra were acquired in positive ionisation mode with auto MS2 fragmentation. Both the standard epothilone B and HPLC collected peak of 40th minute produced a molecular mass of 508.1 Da ($M+H^+$). They also produced the typical MS2 fragments at m/z 420.0 Da and 320.2 Da in the product ion mode. This confirmed the presence of epothilone in *G. lineata* extract. Further confirmation will be made through NMR once enough of the compound is purified.

To understand the chemodiversity of *G. lineata*, we studied the untargeted metabolome of the strain at three different time points. One of the objectives for this was to *identify taxol or its intermediates in the metabolome data. Unfortunately, we failed to find such metabolites.* However, a detailed comparison between the transcriptomic and the secretome data was made to understand the

fungus's lignocellulosic enzyme production capacity, nature of the enzymes, and their possible use in plant biomass hydrolysis. This led to the identification of artemisinin in the untargeted extracellular metabolome. This well characterised antimalarial compound was initially isolated from the plant, Artemisia annua. We also investigated whether monoisotopic mass of the intermediate metabolites of the artemisinin biosynthetic pathway can be predicted from the metabolome data. 10 intermediate compounds were predicted as they were found to match with the metabolites of the artemisinin biosynthesis pathway. *G. lineata* genome was also searched and annotated to identify the genes involved in this pathway. As fungi and plants are distantly related, only three genes could be identified in the *G. lineata* genome with a maximum of 51% identity.

As a basidiomycete and an endophyte to a host plant (i.e., jute) with massive lignocellulosic content, the presence of numerous carbohydrate-active enzymes was expected in *Grammothele lineata*. Considering these, cellulases produced by *Grammothele lineata* were studied extensively in search of an efficient cellulase system applicable in biofuel production. *In silico* analysis of the genome of *G. lineata*, identified a total of 485 genes which were assigned to CAZyme families, and the number of glycoside hydrolases (~53.97%) present was found to be significantly higher than the other families. Secretory proteins were analysed using LC-MS/MS to identify cellulases in cellulase-inducing conditions. A total of 378 proteins were identified from the secretome with high confidence. Among them, 198 proteins were related to metabolism, and 145 proteins were enzymes. dbCAN, a web resource for automated carbohydrate-active enzyme annotation, analysis suggested that a good number of enzymes and associated proteins are secreted, which is the key component for pretreated as well as untreated biomass hydrolysis. More than 70% of secreted total proteins were suggested to be directly related to biomass hydrolysis by Label-Free Quantification (LFQ) using the Protein Discoverer. The richness of CAZymes as well as terpene synthases identified in this endophytic fungus suggests that it is a great candidate to pursue for development into biofuel development platform.

Results Unforeseen in the Original Project:

Initial studies in our lab had revealed that *G. lineata* has the potential to produce a diterpenic polyoxygenated pseudoalkaloid-paclitaxel (taxol), in culture conditions. Therefore, initially the focus of this project was to elucidate the taxol producing pathway functional in *G. lineata.* However, in subsequent studies we failed to isolate taxol from this endofungus. Also, an analysis of *G. lineata* genome failed to pinpoint the genes involved in the biosynthesis of the compound. Even an analysis of the metabolomic data failed to identify taxol or its metabolites. There are reports that the molecular mechanisms required to produce such phytochemicals is likely to be acquired from the plant host. After several generations of growth in axenic conditions, endophytes usually undergo attenuation and thus the endophytes may lose the capacity to produce the compound. Even genome analysis of these endophytes often fails to reveal the complete biosynthetic pathway of the compound.

Publications:

Ehsan, T., Reza, R.N., Das, A., Ahmed, O., Baten, A.K.M.A., Ferdous, A.S., Islam, M.R., Khan, H. Genome and secretome analysis of jute endophyte *Grammothele lineata* strain SDL-CO-2015-1: Insights into its lignocellulolytic structure and secondary metabolite profile. 2020. Genomics, **112(4)**, 2794-2803

COLOMBIA

Title: Phenotypic and functional characterisation of the adaptive immune response during differential progression of COVID-19

Principal Investigator: Maria Teresa Rugeles Lopez, Grupo Inmunovirología. Departamento de Microbiología y Parasitología, Facultad de Medicina, Universidad de Antioquia UdeA, Calle 70 No 52-21, Medellín, Colombia

ICGEB Contract No.: CRP/20/015
ICGEB Reference No.: CRP/COL20-01
Project funded by IILA

Abstract: Given the recent appearance of this SARS-CoV2-pandemic, the current knowledge of the immunological mechanisms triggered against this infection and how they affect the severity of the disease, remain limited. Most evidence indicates that severity of the clinical picture is associated with the viral load and an exacerbated inflammatory response, characterised by a cytokine storm affecting not only the main target organ of the infection, the lung, but also generating systemic alterations that lead to multi-organ failure. In this regard, it is imperative to carry out studies to establish the immunopathogenesis of this infection, identifying the main immune actors that could be favouring severe outcomes. Although the previous experience with SARS in 2002 shed light on some of these pathogenic mechanisms, differences in morbidity and mortality with respect to COVID-19 suggest the presence of qualitatively and quantitatively different immunological abnormalities that are worthy exploring in order to understand the immunopathogenesis of COVID-19.

Objectives:

To characterise alterations in the adaptive immune response observed during SARS-CoV-2 infection in 71 patients from Medellín, Colombia, recruited between November of 2020 and July of 2021. Patients were classified into 4 groups: (i) asymptomatic; (ii) symptomatic outpatients; (iii) hospitalised in ward and (iv) in intensive care unit patients (ICU), and follow-up at 0, 7 and 30 days after recruitment.

Results Obtained:

First, we focused on evaluating the B cells subpopulations in the four study groups, using multiparametric flow cytometry. A significant increase in the percentage of CD19+ cells was observed at day 0 in the ICU and hospitalised patients compared to asymptomatic and symptomatic patients. At days 7 and 30, we observed a reduction in those cells in the UCI and hospitalised patients that was only significant in the hospitalised group. Similarly, we observed a higher plasmablast frequency in the ICU compared to asymptomatic patients at day 0, with a tendency to be reduced after 30 days. In all groups, the plasmablasts, lacking both IgG and IgM were more prevalent. The IgG+ plasmablast proportion tend to be higher at days 7 and 30 in the hospitalised individuals compared to other groups, without reaching statistical significance. The reduction of total B cells could be partially attributed to the reduction of naïve B cells observed on day 7 in hospitalised and ICU individuals and on day 30 in the hospitalised group. Interestingly, an increase of IgM+ memory B cells (MBC) at day 7 was observed. On the other hand, in ICU patients the double-negative B cells were increased at day 30. These findings suggest a differentiation process of the immune response that is more pronounced in hospitalised subjects. We also evaluated NAb titers, and although the response was variable, we observed higher NAb titers in hospitalised and UCI individuals compared with non-hospitalised patients. Interestingly, when we correlated NAb titers with the phenotype of B cells, we found a strong correlation between IgM+ unswitched B cells and plasmablast in asymptomatic individuals. This finding could suggest that the kinetic of NAb-producing cells could be variable, at least in patients with less severe COVID-19. Interestingly, in hospitalised and ICU patients, naïve B cells and IgM-IgG- switched B cells seem to be related with clinical parameters (AST, ALT, total bilirubin, direct bilirubin, blood ureic nitrogen, % saturation, pH, Na+) while IgG+ switched B cells do not. Moreover, conventional inflammation markers such as CRP, D-dimer, and ferritin were positively correlated with WBC count, plasmablasts, neutrophils, and transitional B cells but negatively with lymphocytes. Altogether, these results suggest a differential kinetic of B cells response to SARS-CoV-2. Most likely, in less severe forms of COVID-19, there is an earlier differentiation of B cells towards a phenotype of memory B cells such as IgM+ unswitched B cells and IgM+ MBC, while in severe COVID-19, the admission to hospital matches with the presence of naïve B cells and plasmablasts, all these cells contributing to the inflammatory process. However, over time we noted that only hospitalised individuals turned from immature response to a mature phenotype with the presence of IgM+ unswitched B cells and IgM+ MBC.

KENYA

Title: Deciphering resistance and virulence in sorghum-*Striga* interaction
Principal Investigator: Steven Runo, Kenyatta University, Department of Biochemistry, Microbiology and Biotechnology, The Plant Transformation Laboratory, Thika Road, P O Box 43844-0011 GPO, Nairobi, Kenya. Tel: +254-727-346496, Fax: +254-02-811575, E-mail: smruno@gmail.com, runo.steve@ku.ac.ke
ICGEB Contract No.: CRP/18/001
ICGEB Reference No.: CRP/KEN17-03
Abstract: Sorghum is a major food stable in sub-Saharan Africa (SSA) but its yields are constrained by the parasitic plant Striga that attaches to roots of cereal crops causing severe stunting and loss of yield. Both sorghum and Striga co-evolved in Eastern Africa with no serious threat by the parasite. However, transformation of wild sorghum into elite cultivars through domestication has led to a gradual decline in sorghum resistance, and a corresponding increase in Striga virulence. In this ICGEB-CRP project, we sought to expand the genetic basis of cultivated sorghum to cope with evolving Striga virulence in order to build durable and broad-spectrum resistance. Our hypothesis hinged on: (i) our previous findings that revealed wild sorghum accessions are important reservoirs of Striga resistance genes and (ii) emerging literature that Striga is able to evade host immunity using effector molecules. The project achieved following outputs: (i) development of tissue culture protocols for the obligate parasitic plant Striga hermonthica; (ii) elucidation of gene networks for sorghum-Striga interactions; (iii) establishment of a platform for genetic transformation of sorghum for Striga resistance; (iii) identification of new Striga resistant sorghum adapted to Africa agro-ecologies; (iv) leveraging new partnerships for establishment of a sorghum genome-editing platform.
Objectives:
In this application, we sought to expand the genetic basis of cultivated sorghum to cope with evolving Striga virulence in order to build durable and broad-spectrum resistance. We wanted to achieve this by developing resistance in sorghum against Striga based on interactions between effectors, virulence genes from Striga and resistance genes from sorghum. Our work was to provide critical information on the resistance mechanism of sorghum to Striga and how that resistance can be maintained. Outputs from this project are directly applicable in SSA and enable farmers to grow Striga resistant sorghum in the short-term.
We were guided by two specific objectives:
(i) To determine the role of Pathogenesis-Related Proteins in the sorghum-Striga interaction,
(ii) To determine the role of effectors in the sorghum-Striga interaction.
Results Obtained:
To determine the underlying genetic course of this resistance, we used RNA sequencing to determine genes, in wild sorghum, that are differentially expressed at early and late Striga infection and compared their profile to those of susceptible cultivated sorghum. In addition, we compared the profile of differentially expressed genes between Striga infecting wild and cultivated sorghum. We found that more genes were differentially expressed in wild sorghum upon Striga infection and that more Striga genes were differentially expressed when the infection was on wild sorghum. These findings suggest that wild sorghum has more genetic diversity to cope with Striga and that more genes in Striga are required to overcome resistance from the host. RNA sequencing data further led us identify a set of candidate Striga resistance genes from wild sorghum as well as a rapporteur of molecules (effectors) that may be aiding Striga to overcome the innate immunity of its hosts.
In summary, we found the following genes as important regulators of resistance in sorghum:
(i) dehydration-responsive element-binding (DREB) protein/C-repeat binding factors (CBFs), which belong to APETALA2 (AP2) family transcription factors. In our analysis, DREB was downregulated in susceptible but upregulated in resistant varieties.
(ii) Universal Stress Protein A. This gene was also upregulated in resistant varieties relative to susceptible varieties and has been demonstrated to confer resistance against a broad range of pathogens.
(iii) Cytokinin-Activated Transcription Factor ARR2. This gene confers plant immunity via the Non expressor of pathogenesis related protein 1 (NPR1)-dependent salicylic acid signaling in Arabidopsis.
(iv) Leucin rich repeat receptor like genes. Two LRR-like were also significantly differentially expressed. LRR point to programmed cell death resistance. On the virulence component of Striga-sorghum interaction. The most prominent genes were the Pectin methylesterase inhibitors (PMEI) that work to inhibit Pectin methylesterases (PMEs) that catalyse the demethylesterification of the homogalacturonan domains of pectin in the plant cell wall.
To further elucidate the intricate host-parasite interactions between Striga and sorghum, we sought to carry out functional validation of resistance and virulence genes. To achieve this goal, we developed efficient protocols for Striga *in vitro* culture in order to achieve optimal growth and proliferation of Striga plants. This is a necessary step for all subsequent *in vitro* culture based experiments that require aseptic Striga tissue. In addition, we required a protocol that will lead to

production of a large amount of Striga somatic embryos that can be efficiently regenerated. For many tissue culture protocols, role of growth regulators is critical for somatic embryogenesis and regeneration. We therefore varied concentrations of the auxin Naphthaleneacetic acid (NAA) and cytokinin 6-Benzylaminopurine (BAP). These experiments led us to establish further protocols for Striga somatic embryogenesis, regeneration and organogenesis. To analyze the Striga resistance component in sorghum, we developed a sorghum transformation platform using candidate resistance genes.

Results Unforeseen in the Original Project:

To increase the efficiency of candidate gene validation we are now taking a genome editing approach. This has been made possible through establishment of a strategic partnership with Corteva Agriscience, leaders in genome editing protocols, and Pennsylvania State University. This partnership allowed us to get proof-of-concept that genome editing can be used as a Striga-sorghum functional genomics tool and also as a strategy for introducing resistance against Striga. This proof was obtained following on previous knowledge that Striga germination occurs in response to stimulation by the plant hormone strigolactone and that Striga resistance in sorghum occurs due to a natural mutation in the loci called *LOW GERMINATION STIMULANT1* (*LGS1*) that prevent them from producing the germination stimulant. CRISPR/Cas9 was used to precisely introduce mutations in a farmer popular sorghum variety called Marcia in the *LGS1* loci. These Striga resistant gene-edited material have been developed and will be evaluated at Kenyatta University.

In addition to genome editing we have also embarked on a screening a large population of sorghum for Striga resistance based on mutation on the LGS1 loci. To identify more targets for CRISPR we have taken a Genome wide association studies (GWAS) approach using Genotyping-by-sequencing (GBS) based Single Nucleotide Polymorphism (SNPs). This work led us to identify new sorghum varieties harboring pre-attachment resistance against Striga. We were also able to able to determine new genetic loci underpinning the resistance.

Publications:

Waweru, D., Kuria, E., Bradley, J., Scholes, J., Runo, S. Tissue culture protocols for the obligate parasitic plant *Striga hermonthica* and implications for host-parasite co-cultivation. 2019. Plant Cell Tiss. Organ Cult. **138,** 247–256

Bellis, E.S., Kelly, E.A., Lorts, C.M., Gao, H., DeLeo, D.L., Rouhan, G., Budden, A., Bhaskara, G.B., Hu, Z., Muscarella, R., Timko, M.P., Nebie, B., Runo, S.M., Chilcoat, N.D., Juenger, T.E., Morris, G.P., dePamphilis, C.W., Lasky, J.R. Genomics of sorghum local adaptation to a parasitic plant. 2020. Proc. Natl. Acad. Sci. USA, **117 (8),** 4243-4251

Mallu, T.S., Mutinda, S., Githiri, S.M., Odeny, D., Runo, S. New pre-attachment Striga resistant sorghum adapted to African Agro-ecologies. 2021. Pest Management Science (in press)

KENYA

Title: Characterisation of the SARS-CoV-2 virus and antibodies
Principal Investigator: Tindih Sheltone Heshborne, Biological Sciences Laboratory, Department of Biological Sciences, School of Pure and Applied Laboratory, Machakos University, Kenya. Tel: +254715831853; E-mail: tindih.heshborne@mksu.ac.ke
ICGEB Contract No.: CRP/20/011
ICGEB Reference No.: CRP/KEN20-01
Abstract: The novel coronavirus disease 2019 (COVID-19) and the SARS CoV-2 outbreak was first announced around December 2019, in Wuhan, China and officially declared a pandemic by WHO on 30 January 2020. Since then, it has been evolving faster, and the disease has tremendously spread across the globe with infections currently standing at 248,824,610 of infected cases, while mortalities is at 5,037,026 and 225,450,289 recovered cases (figures as of 4 November 2021). SARS-CoV-2 infected cases present symptoms like fever, fatigue, dry cough, and dyspnoea; with or without nasal congestion, runny nose or other upper respiratory symptoms. While the immediate interventions need to focus more on slowing or stopping the pandemic, the needs to collect data that will help broad management of the disease is necessary. Currently there are vaccines which can slow down the pathogenic stage of the disease but in the long run vaccines or drugs that can block viral invasions of the cells and replications are necessary. To achieve that goal we will need to understand viral genetics, host immune responses (including both cellular and humoral antibodies responses), as well as the viral reservoirs in both domestic and wild animals that could acts as future source of infections. Currently there are a number of serological and molecular based studies, which have shown SARS CoV-2 exposure to pets such as cats, dogs and other companion animals, such as farmed minks in Europe, USA and China. However, most of these studies have either looked at experimentally infected animals or susceptibility testing through introduced virus. There are few data to support a naturally exposed animal to SARS COV-2 virus. It is with that perspective that we designed this study to assess possible status or exposure of the virus in animal population in Kenya by developing an antibody-based ELISA and using it to assess the sero-status of the animals as well comparing those results with a spike RBD antigen specific commercial kit.
To help us assess the extent of the SARS COV-2 exposure to the animal populations in Kenya, we collected camels sera (both pre- and post outbreak sera), cats, dogs and a few bats samples. We then used both commercial kit ELISA based on spike specific RBD and also developed an in-house assay based on crude SARS COV-2 lysate and a modified Amanat et al based ELISA protocol.
Our results indicated SARS COV-2 like antibodies in camels, cats, dogs and bats with varying prevalence. The implications on our finding on the origin of the virus, neutralisation capacity of this antibodies and the possibility on the presence of the other Coronaviruses in Kenya is thus discussed in this grant.
In conclusion, we confirm that it is possible to use crude lysate ELISA to recognise and increase sensitivity of the ELISA test. Crude lysate includes other SARS COV-2 antigens i.e., S1, Spike RBD, NP, Heamaglutinin and M that can help reduce false negatives. In conclusion, there already exists SARS COV-2 viral exposure to the camels, cats, dogs and bats. Whether this is of natural origin or a case of human to animal transmissions, is still unclear. It will be important to evaluate this further.
Objectives:
Our specific objectives were:
(i) Isolation and characterisation of SARS CoV-2 virus in animal samples and compare with human virus;
(ii) Serological characterisation of SARS CoV-2 virus;
(iii) Characterisation of the SARS-Cov-2 antibodies.
Results obtained:

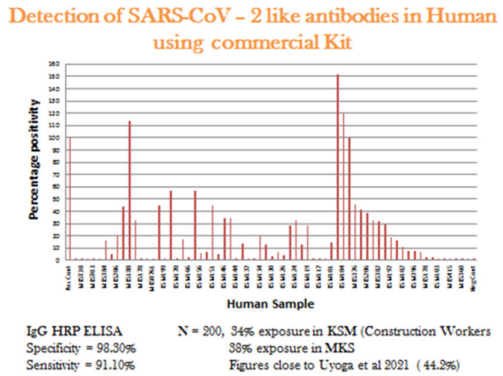

Fig 1. Presence of SARS CoV- antibodies in Kenya 92 counties serosurveillance). The estimates exposure at 34% higher than the RT-PCR data.

Fig.2 A comparison of the distribution of SARS CoV-2 like antibodies in camel sera determined both by a commercial kit (n=19) and by the crude lysate ELISA (n=145), and expressed as a percentage of the positive control serum (percent positivity). White circles show the medians; box limits indicate the 25th and 75th percentiles as determined by R software; whiskers extend 1.5 times the interquartile range from the 25th and 75th percentiles; polygons represent density estimates of data and extend to extreme values. This finding of the presence of SARS COV-2 like antibodies in Camels in Kenya based on our crude lysate ELISA, was corroborated by the results obtained using the commercial kit based on the Spike specific RBD antigen (Figure x). It is important to note that in that the crude lysate ELISA potentially includes up to 4 major antigens that could be seen by the antibodies, as opposed to the single antigen in the commercial kit. In addition, the number of camel sera analysed using the crude lysate were nearly ten times more than those analysed using the commercial kit. Notwithstanding the differences outlined above, figure x shows that the seroprevalence determined by both assays was still high even at the stringent PP threshold of 20%.

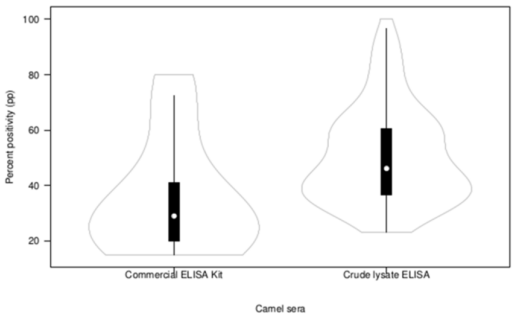

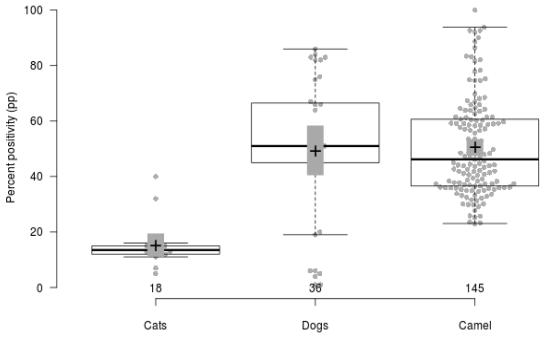

Fig 3. Prevalence of SARS COV-2 like among cats, dogs and camels in Kenya as assessed using the crude lysate ELISA developed herein. Center lines show the medians; box limits indicate the 25th and 75th percentiles as determined by R software; whiskers extend 1.5 times the interquartile range from the 25th and 75th percentiles, outliers are represented by dots; crosses represent sample means; bars indicate 95% confidence intervals of the means; data points are plotted as open circles. Results are given as a percentage of the positive control serum (percent positivity, PP). The data interpretation was based on the stringent cut-offs (20% PP) for negative or positive ELISA results.

MALAYSIA

Title: D-amino acids as potential modulators of age-related functional decline in natural and accelerated aging

Principal Investigator: Reena Rajasuriar, Department of Medicine, Faculty of Medicine, University of Malaya, Jalan University, 50603 Kuala Lumpur, Malaysia. Tel: +603-79676617, Fax: +603-79491751

ICGEB Contract No.: CRP/18/003
ICGEB Reference No.: CRP/MYS17-05

Abstract: D-amino acids (AA), which is a mirror-image of L-AA, have been associated with age-associated diseases including Alzheimer's, chronic kidney disease, Parkinson's disease and frailty; raising speculation that D-AAs may contribute to the aging process. D-AAs are abundantly found in bacterial cell wall structure and intestinal microbial products and the translocation of bacterial products from intestine to the circulation has been shown to occur in many age-associated diseases and in HIV disease, a disease model for accelerated aging. The breakdown of D-AAs by D-amino acid oxidase (DAO) enzyme produces hydrogen peroxide, which may contribute to increased oxidative stress in the tissue microenvironment, leading to eventual organ damage/decline. We found that D-aa measured in plasma was significantly correlated with age in individuals with and without HIV disease and significantly associated with surrogate markers of liver and kidney disease. Additionally, D-aa were correlated with markers of inflammation suggesting their potential role as a biomarker of inflammaging. *In vitro* mechanistic studies in HepG2 cell lines, confirm that the breakdown of D-aa by DAO generates hydrogen peroxide, albeit variably and leads to the activation of NF-kB and the subsequent release of inflammatory cytokines in cell supernatant. Our findings collectively suggest the potential role of D-aa as a previously unrecognised biological entity associated with the process of inflammaging in humans.

Objectives:

(i) To explore the accumulation of D-AAs and its association with geriatric conditions and immunological aging in HIV-infected and uninfected individuals;
(ii) To elucidate the mechanistic pathways affected following exposure to D-AAs through cell-based assays.

Results Obtained:

The concentration of 4 common D-AAs, namely D-Ser, D-proline (D-Pro), D-alanine (D-Ala) and D-asparagine (D-Asn), have been quantified using three dimensional-HPLC in plasma samples of 60 HIV-infected and 59 HIV-uninfected controls. The markers of immune activation and inflammation namely, sCD14, IL-6, TNF-α, IL-1B, sCD163 and hsCRP as well as markers of intestinal permeability I-FABP, LBP and zonulin have been measured in all samples using platforms of ELISA and ELLA. Activity of IFN-gamma-induced indolamine-2,3-deoxygenase, as represented by ratio of kynurenine and tryptophan concentrations (K/T ratio) in the plasma, has also been quantified by LC-MS/MS. Cellular markers of T-cell activation (CD38+, HLA-DR+) and senescence (CD57+, CD28-) have also been quantified by flow cytometry in cryopreserved peripheral blood mononuclear cells.

In our findings we have found that the concentrations of D-Asn, D-Ser, D-Ala and D-Pro increased as both HIV-infected participants and HIV-uninfected controls were older in age. The concentration of D-AAs was also significantly associated with clinical markers of kidney, liver organ function and with the composite Veterans Aging Cohort mortality risk scores in both the HIV-infected and uninfected controls. In addition, specific D-AAs were associated with inflammation markers (TNF-α, K/T ratio and sCD14), suggesting the potential role of D-AAs as putative markers of inflammaging. Furthermore, a higher concentration of D-AAs was observed in HIV-infected individuals presenting with various geriatric conditions (cognitive impairments, urinary incontinence, functional impairment, polypharmacy and polypathology). However, these differences were no longer significant when adjusted for age implying that exposure to D-AAs in individuals with functional aging phenotypes were modulated by age. We did not find a consistent correlation between D-AAs in plasma with direct markers of increased gut permeability and damage in HIV-infected participants to suggest that the source of D-AAs in plasma is a result of microbial products translocating into the systemic circulation. In short, D-AAs may likely play a role in driving multiple organ dysfunction and immune activation in HIV-infected and uninfected controls but are unlikely to be driven by microbial translocation.

To understand the effect of D-AAs on cells, we investigated the activity of DAO following exposure to D-aa to HepG2 cells by measuring the production of H_2O_2. D-AAs is metabolised by DAO and generates hydrogen peroxide (H_2O_2), but variable kinetics were detected with the two D-aa tested *in vitro*. There was an increased in H_2O_2 production for D-Ala, but reduced production following D-Ser treatment. We further determined the levels of DAO gene and protein expression, to understand the difference in H_2O_2 production for different treatment. We found that DAO gene expression was upregulated for D-Ala treatment but downregulated when the cells were treated with D-Ser. These results were consistent with the levels of DAO protein expression measured by Western blot following D-Ala and D-Ser treatment. We next explored if the production of H_2O_2 following D-aa exposure

modulates NF-kB protein expression. We analysed activated NF-kB protein expression following D-AAs treatment using Western blot and found that activated NF-kB protein levels in HepG2 were decreased initially in low concentrations of Daa but increased significantly in high D-aa concentrations after treatment with both D-Ser and D-Ala. We also analysed the cell culture supernatants for inflammatory cytokine secretion. The concentrations for TNF-α and IL-8 increased for both D-Ala and D-Ser treatment. However, IL-6 was not detectable in the supernatants. Taken together, these results suggest that the breakdown of D-Ser and D-Ala by DAO is associated with the production of hydrogen peroxide leads to NF-kB activation and cytokine release, consistent with that observed in plasma samples of aging individuals.

Results Unforeseen in the Original Project:

Different D-AA may affect cellular response differently as we found in our experiments that the regulations of DAO gene and protein expression, as well as the hydrogen peroxide production, by D-Ser and D-Ala were different. However, both amino acids were found to be metabolised by DAO enzyme as found in previous studies and led to the production of H_2O_2. The mechanistic pathway behind this difference is unclear and a thorough investigation on the cellular pathway involved is needed. Additionally, we anticipated that the levels of D-aa will be higher in plasma concentrations of people living with HIV, a disease model for accelerated aging as a result of increased microbial translocation in this group. However, HIV status was found to not be independently associated with concentration of circulating D-aa and that markers of microbial translocation was not associated with D-aa levels. D-aa could still be associated with changes in metabolites produced gut microbiome, as aspect which was not explored in our study and worth investigating in future work.

MALAYSIA

Title: Nanomaterials based-Genosensor (Nano-GS) for improved detection method of SARS-CoV-2 RNA as rapid COVID-19 diagnosis strategy

Principal Investigator: Tan Ling Ling, Southeast Asia Disaster Prevention Research Initiative (SEADPRI-UKM), Institute for Environment and Development (LESTARI), Universiti Kebangsaan Malaysia, 43600 UKM Bangi, Selangor Darul Ehsan, Malaysia. Tel: +601-2-2321300, Fax: +603-89275629, E-mail: lingling@ukm.edu.my

ICGEB Contract No.: CRP/20/030
ICGEB Reference No.: CRP/MYS20-03

Abstract: Colorimetric RNA biosensor was developed by using cysteamine-stabilised gold nanoparticles (cysAuNPs) as the optical probe for assay of COVID-19 (SARS-CoV-2) RNA. The cysAuNPs aggregated in the presence of DNA probes via electrostatic interaction between positively charged cysteamine ligands and negatively charged sugar-phosphate backbone of DNA, whilst in the presence of target RNAs, the specific recognition between DNA probes and targets negated the electrostatic interaction between DNA probes and cysAuNPs, leading to dispersed particles. This rendered a remarkable shifting in the surface plasmon resonance on the basis of visual colour change of the RNA biosensor from red to purplish hue at the absorption wavelength of 765 nm. Optical evaluation of SARS-CoV-2 RNA by means on UV-vis absorption transduction of the RNA biosensor based on cysAuNPs optical sensing probes demonstrated rapid response at 30 min with high sensitivity, good linearity and high reproducibility across COVID-19 RNA concentration range of 25-200 nM, and limit of detection at 1.2 fM. The optical RNA biosensor shows high selectivity towards assay of SARS-CoV-2 RNA compared to MERS-CoV and SARS-CoV viral sequences.

Objectives:

(i) To synthesise and characterise the physical and chemical properties of cysAuNPs substrate by UV-Vis spectrophotometer, field emission scanning electron microscopy (FESEM) and Fourier-transform infrared spectroscopy (FTIR);
(ii) To evaluate optical and electrochemical responses of RNA-responsive cysAuNPs-based nanogenosensor by means of reflectance spectrophotometry, differential pulse voltammetry (DPV) and electrochemical impedance spectroscopy (EIS) for biorecognition of SARS-CoV-2 RNA;
(iii) To develop an embedded electronic reader consisting of software/Apps that are used for parameter setting and display from RNA biosensor;
(iv) To validate the electrochemical and optical responses of the developed RNA biosensors in RNA for patient's secretions tested to be positive for COVID-19 infection, and compare with the results obtained with qPCR reference method.

Results Obtained:

(i) Characterisation of the as-prepared colloidal cysAuNPs

The average size of the as-prepared cysAuNPs was characterised by transmission electron microscopy (TEM) and UV-vis spectrophotometry analysis. The cysAuNPs was synthesised by the reduction of gold salt ($HAuCl_4$) with sodium borohydride ($NaBH_4$) as the reducing agent in the presence of cysteamine dihydrochloride. The UV-vis spectrophotometric spectrum of the cysAuNPs colloids exhibits a maximum absorption peak at 542 nm, which indicates the formation of small monodisperse gold nanoparticles. The surface plasmon resonance phenomenon causes an absorption of light in the blue-green portion of the spectrum (~450 nm) whilst red light (~700 nm) is reflected, and yielding a red ruby colloidal gold [16,17]. TEM analysis revealed that the as-synthesised cysAuNPs were spherical in shape and had an average particle size of 22.18±2.00 nm.

(ii) The principle of cysAuNPs-based reflectometric biosensor for RNA detection

The as-prepared red ruby colloidal cysAuNPs gave a maximum reflectance signal at the wavelength of 639 nm, which was attributed to the electrostatic repulsion between cationic cysAuNPs, whereby each gold nanoparticle was repelled from the other by an electrostatic force and that forming colloidally stable monodisperse gold nanoparticles. Upon introduction of 300 nM DNA probes, the cysAuNPs colloidal suspension turned from red to purple hue based on electrostatic attraction-induced aggregation of the gold nanoparticles. A remarkable reflectance response attenuation was observed during anionic DNA probe immobilisation on the cationic cysAuNPs, which was ascribed to the purple-coloured DNA probe-cysAuNPs bioprobe that possessed a darker coloration compared to the red-coloured colloidal cysAuNPs, thereby considerably reduced the reflected light intensity. In view of the affinity of the immobilised DNA probe towards binding with its target RNA is higher than the cationic cysAuNPs, hybridisation between DNA probe and target RNA neutralised the electrostatic interaction between anionic DNA probe and cationic cysAuNPs, leading to redispersion of the cysAuNPs and heightening the reflectance response. However, the level of reflectance intensity enhancement of the optical RNA biosensor based on cysAuNPs was depending on the loading of the target RNA. The purple-coloured DNA probe-cysAuNPs bioprobe changed to reddish purple hue upon reaction with low concentration of target RNA due to only small number of negatively charged immobilised DNA probes were being detached from the positively charged cysAuNPs for hybridisation

with the target RNA, and the remaining large amount of cationic DNA probes were remained electrostatically bound to the cationic cysAuNPs to induce aggregation of the gold nanoparticles. However, further loading of high RNA concentration in the DNA probe-cysAuNPs colloids, a distinct colour change from reddish purple to dark red was perceived as most of the immobilised DNA probes were detached from the cysAuNPs as a result of competitive binding of the DNA probe to the cysAuNPs and target RNA. Because of the specific recognition between DNA probes and target RNAs, it negated the electrostatic attraction between DNA probes and cysAuNPs. The positive surface charge of the cysAuNPs repelled each other and rendering redispersion of the gold nanoparticles.

(iii) Establishing calibration curve for the determination of viral RNA

Different concentrations of target RNA were prepared between 25 nM and 300 nM and analysed with the optical RNA biosensor in order to determine the linear concentration response range of the cysAuNPs-based reflectance biosensor. The purple coloration of the cysAuNPs-based RNA biosensor has the lowest reflectance intensity at 639 nm compared to its original unmodified red ruby cysAuNPs. Hybridisation between DNA probe and target RNA between 25 nM and 75 nM has heightened the reflectance response at 639 nm due to electrostatic repulsion-induced redispersion of the gold nanoparticles, and turned to reddish purple that conferred a brighter coloration. However, loading of the target RNA concentration above 75 nM i.e., between 100 nM and 250 nM, the RNA biosensor's maximum reflectance signal shifted to 765 nm as the DNA-coated colloids changed to dark red hue when like charges repelled each other. Over loading of the target RNA into the DNA probe-cysAuNPs colloids at 300 nM RNA, however, has shifted back the maximum reflectance intensity at 639 nm as the presence of a large amount of RNAs, which consist of ribose sugar phosphate backbones have induced an electrostatic attraction between the highly negatively charged RNAs and highly positively charged cysAuNPs. In view of the reflectance peaks of the cysAuNPs-based RNA biosensor at 765 nm provided a wide RNA concentration detection range with well-defined optical reflectance signal separation towards changes of RNA concentration, therefore it was opted as the working reflectance wavelength in the determination of viral RNA. The linear response range of the optical RNA biosensor was determined to be between 75 nM and 300 nM target RNA at 765 nm by using 30 nM DNA probe in the presence of 95.0 µL colloidal cysAuNPs.

Publication:

Nadiah, I., Nur Diyana, J., Ling Ling, T., Nurul Yuziana, M.Y. A review on the development of gold and silver nanoparticles-based biosensor as a detection strategy of emerging and pathogenic RNA Virus. 2021. Sensors **21**. 5114

PAKISTAN

Title: Development of recombinant vaccines to combat inclusion-body hepatitis-hydropericardium syndrome in poultry

Principal Investigator: Aamir Shehzad, Senior Scientist, Drug Discovery and Structural Biology Laboratory, Health Biotechnology Division, National Institute for Biotechnology and Genetic Engineering (NIBGE), Jhang Road, Faisalabad 38000, Pakistan. Tel: +92-331-8894292, E-mail: aamiruopbbt@yahoo.com

Former Principal Investigator: Moazur Rahman, School of Biological Sciences, University of the Punjab, Lahore, Pakistan. Tel: +92-42-35953122, E-mail: moaz.sbs@pu.edu.pk

ICGEB Contract No.: CRP/17/011

ICGEB Reference No.: CRP/PAK17-01

Abstract: The poultry industry plays an important role in meeting the food demand of the growing world population. One of the viral diseases which has inflicted significant damages to the poultry industry is inclusion-body hepatitis-hydropericardium syndrome (IBH-HPS) which is caused by Fowl adenovirus serotype-4 (FAdV-4). Conventional vaccines available in the market have failed to provide complete protection against IBH-HPS in chickens. In the current project, modern vaccine candidates were produced for providing complete protection against IBH-HPS in chickens. To this end, five immunogenic regions (penton base$^{77-528}$, penton base$^{143-474}$, penton base$^{143-385}$, penton base$^{1-225}$ and penton base$^{420-470}$) on the FAdV-4 penton base protein were selected through bioinformatics approaches, expressed using recombinant means, purified through chromatographic techniques, characterised by biophysical approaches, and evaluated for protective efficacy against pathogenic FAdV-4 challenge in chickens. The data reveal that two subunit vaccine candidates (penton base$^{143-474}$ and penton base$^{143-385}$) provide complete (100%) protection against IBH-HPS in chickens. Penton base$^{143-474}$ is the only variant that folds as pentamer (similar to other penton base proteins). Both the subunit vaccine candidates can be produced in bulk for conducting large-scale field trials and commercialization.

Objectives:

The main objective of this research project was to obtain immunogenically active and thermally stable forms of penton base in sufficient amounts that could be exploited as vaccine candidate to combat IBH-HPS in chickens. This was achieved through a number of objectives:

(i) Computational and bioinformatics analysis of penton base to identify potent immunogenic variants/regions for vaccine development;

(ii) Cloning and expression of potent immunogenic variants/regions of penton base and their optimisation studies for over-expression;

(iii) Purification and structural characterization of potent immunogenic variants/regions of penton base;

(iv) Immunogenic analyses of potent immunogenic variants/regions of penton base to check their potential as recombinant vaccine.

Results Obtained:

During the current project, computational and bioinformatics analyses of the FAdV-4 penton base protein were first performed to identify immunogenic regions. Various bioinformatics tools were used to predict B- and T-cell epitope on the penton base capsid protein, taking into account the sequence and the structural information of the target (penton base) protein. Five immunogenic regions (penton base$^{1-225}$, penton base$^{77-528}$, penton base$^{143-385}$, penton base$^{143-474}$, and penton base$^{420-474}$) were finally selected for conducting immunisation studies in chickens. Penton base$^{1-225}$ was selected for immunisation studies since it contains multiple linear and discontinuous B-cell epitopic regions. As the structural and biochemical analyses of the penton base protein revealed that the N-terminal region contains a disordered loop (from position 1 to 76) which is prone to cleavage by proteases, penton base$^{77-528}$ was selected as a stable vaccine candidate for immunisation studies. Penton base$^{143-474}$ and penton base$^{143-385}$ were selected for immunisation studies since these regions contain multiple T-cell epitopes. Owing to its surface-exposed nature on the full-length penton base, a short peptide epitopic region, penton base$^{420-470}$, was selected for the hepatitis B virus (HBV) core protein-based vaccine design strategy that involves presentation of the immunogenic region to the immune system of the host in the form of virus-like particles.

The selected subunit vaccine candidates (penton base$^{1-225}$, penton base$^{77-528}$, penton base$^{143-385}$, penton base$^{143-474}$), in addition to the full-length penton base protein, were then heterologously expressed in the bacterial (*Escherichia coli*) expression system using a pET (pET28a-Pres) plasmid under the control of an isopropyl β-D-1-thiogalactopyranoside (IPTG)-inducible T7 promoter. It was observed that all penton base variants, except penton base$^{1-225}$, were expressed in a soluble form in *E. coli*. The penton base$^{1-225}$ variant was predominantly expressed in the form of inclusion bodies in *E. coli*, prompting us to solubilise and refold the target protein from inclusion bodies. Similar to the penton base$^{1-225}$ variant, the virus-like particle vaccine candidate (penton base$^{420-474}$) was also

expressed in the form of inclusion bodies in *E. coli*, and was subjected to on-column refolding during affinity chromatography.

The expressed vaccine candidates, and the full-length penton base protein, were successfully purified through affinity chromatography using Ni-NTA columns. It was found that the purification yield of the recombinant proteins (His_6-PreS-penton $base^{1-225}$, His_6-PreS-penton $base^{77-528}$, His_6-PreS-penton $base^{143-474}$, and His_6-PreS-penton $base^{143-385}$) was 3-fold, 8-fold, 15-fold, and 17-fold higher than the full-length penton base protein, respectively. An improved purification yield of His_6-PreS-penton $base^{77-528}$, His_6-PreS-penton $base^{143-474}$, and His_6-PreS-penton $base^{143-385}$ could be due to a reduced disorder in the penton base variants as analysed through circular dicroism (CD) spectroscopy, revealing a lower CD signal (ellipticity) in the case of the penton base variants compared to the full-length penton base protein. The gel filtration analysis revealed that, among the purified subunit vaccine candidates, only His_6-PreS-penton $base^{143-474}$ was predominantly found in a pentameric form in solution, similar to the native FAdV-4 penton base protein. Interestingly, the removal of the polyhistidine tag (His_6) upon cleavage with the HRV 3C protease enzyme shifted the equilibrium in the favor of the monomeric form of the protein, suggesting that the polyhistidine tag plays an important role in stabilising the pentameric state of His_6-PreS-penton $base^{143-474}$ in solution. The pentameric nature of His_6-PreS-penton $base^{143-474}$ was also confirmed through dynamic light scattering (DLS) and electron microscopy (EM). In order to produce crystals for structural studies through X-ray crystallography, His_6-PreS-penton $base^{143-474}$ was subjected to crystallisation trials. However, our attempts to crystallise His_6-PreS-penton $base^{143-474}$ and other penton base variants have so far remained unsuccessful.

The protective efficacy of the purified penton base variants, and the full-length penton base protein, was evaluated through immunisation studies in chickens, and was compared with a commercially available inactivated FAdV-4 vaccine (Angara NIAB). Similar to the full-length penton base protein and the commercial vaccine, His_6-PreS-penton $base^{1-225}$ provided 50% protection against a pathogenic FAdV-4 challenge. In contrast, His_6-PreS-penton $base^{77-528}$, His_6-PreS-penton $base^{143-474}$, and His_6-PreS-penton $base^{143-385}$ provided complete (100%) protection against IBH-HPS in chickens. The lowest protection was offered by the virus-like particle vaccine candidate (penton base epitopic region (Phe420-Pro474)) which provided 12.5% protection against the disease in chickens.

The analysis of the antibody titer of the collected serum samples in an indirect enzyme-linked immunosorbent assay (ELISA) using the purified FAdV-4 virus as a coating antigen revealed that the selected immunogenic regions (Cys143-Pro474 and Cys143-Thr385) can be readily recognised by the virus, suggesting that both the immunogenic regions (Cys143-Pro474 and Cys143-Thr385) are exposed on the surface of the intact FAdV-4 virus. Moreover, a significantly high purification yield of His_6-PreS-penton $base^{143-474}$ and His_6-PreS-penton $base^{143-385}$ make them suitable as modern (recombinant) vaccines to combat IBH-HPS.

Results Unforeseen in the Original Project:

It was observed that the presence of a polyhistidine tag at the N-terminus stabilises the pentameric state of His_6-PreS-penton $base^{143-474}$ in solution, and the equilibrium is shifted in the favor of the monomeric state upon cleavage of the polyhistidine tag from the recombinant protein, which is an unexpected and surprising finding.

Publications:

Aziz, F., Tufail, S., Shah M.A., Salahuddin Shah, M., Habib, M., Mirza, O., Iqbal, M., Rahman, M..*In silico* epitope prediction and immunogenic analysis for penton base epitope-focused vaccine against hydropericardium syndrome in chicken. 2019. Virus Res. **273**, 197750

Tufail, S., Shah, M.A., Zafar, M., Asif, T.A., Shehzad, A., Shah, M.S., Habib, M., Saleemi, M. K., Muddassar, M., Mirza, O., Iqbal, M., Rahman, M. Identification of potent epitopes on hexon capsid protein and their evaluation as vaccine candidates against infections caused by members of *Adenoviridae* family. 2021. Vaccine **39**, 3560-3564

Tufai, S., Shah, M.A., Zafar, M., Iqbal, M., Ali, A., Shehzad, A., Rahman, M. Tools for prediction and validation of epitopic regions on protein targets for vaccine development and diagnostics. 2021. In: Frontiers in Protein and Peptide Sciences (Frontiers in Molecular Pharming), Benham Science Publisher, **2**, 1-29. ISSN (Online):2213-9877, ISSN (Print): 2589-2924, ISBN (Online) 978-981-5036-66-3, ISBN (Online) 978-981-5036-67-0

RUSSIA

Title: Role of zinc-driven interaction of amyloid-beta with neuronal proteins in Alzheimer's disease
Principal Investigator: Sergey A. Kozin, Engelhardt Institute of Molecular Biology, Russian Academy of Sciences, Vavilova str. 32, Moscow 119991, Russia. Tel: +7-499-1359824; Fax: +7-499-1351405; E-mail: kozinsa@gmail.com
ICGEB Contract No.: CRP/17/012
ICGEB Reference No.: CRP/RUS17-01
Abstract: Endogenous amyloid-beta (Aβ) is normally a monomeric component of biological fluids, however, it forms soluble neurotoxic oligomers in Alzheimer's disease, and also accumulates as insoluble polymeric aggregates (amyloid plaques) in the brain tissues. Earlier, we determined that zinc-dependent oligomers of certain isoforms of Aβ are capable of triggering pathological aggregation of endogenous Aβ, as well as causing neuronal death. There is evidence that formation of zinc-dependent oligomers of Aβ is dependent on its rigidly structured segment 11-14. This site provides two coordination bonds for one zinc ion and through symmetric coordination of this ion a second Aβ molecule forms one of the two zinc-dependent interfaces in each molecule of Aβ in oligomers. By means of the 11-14 site Aβ is able to form zinc-bound interfaces not only in Aβ homo-oligomers but also in zinc-induced Aβ interactions with other endogenous proteins in which there are sites similar in structure to the site 11 -14 of Aβ. The project has addressed the role of zinc-driven interaction of Aβ with neuronal proteins in Alzheimer's disease.
Objectives:
(i) Determination of potential sites of zinc-dependent interaction between isoforms of Aβ and neuronal proteins associated with the progression of Alzheimer's disease;
(ii) Determination of the structural and functional properties of zinc-linked intermolecular complexes formed by Aβ isoforms and partner proteins and/or their fragments;
(iii) Testing on animal AD models (*C. elegans*) of possible therapeutic effect of specific inhibition of zinc-dependent interactions of Aβ with partner proteins.
Results Obtained:
(i) 3D models of the Aβ(1-42) and isoAsp7- Aβ(1-42) structure with predetermined structure of site 11-14 (bearing a zinc ion chelated by Glu11 and His14) were used as ligands for molecular docking. As target proteins interacting with above Aβ isoforms we have probed Na,K-ATPase, α4β2 nicotinic acetylcholine receptor (α4β2-nAChR), and sheep prion (PrP^C). Computer docking of ligands and target proteins was done using four servers (Gramm-x, ClusPro, SwarmDock, Zdock). Scoring, analysis and ranking of protein-protein docking models was performed using QASDOM Server (http://qasdom.eimb.ru/Qasmod.html). Unlike the PrP^C and α4β2-nAChR, for the Na, K-ATPase there were no suitable sites for zinc-induced interactions with Aβ. The simulations performed show that, the interaction interfaces remain similar for Aβ and isoAsp7- Aβ. Residues His64 and His72 from octarepeat sequence of flexible N-terminal fragment of ovine PrP^C are the most like ligands for zinc coordination on the interface with Aβ and isoAsp7- Aβ. Complexes of Aβ and isoAsp7-Aβ with C-terminal fragment of ovine PrP^C are mediated by PrP^C residues His143 and Asp147. Complexes of Aβ and isoAsp7-Aβ with α4β2-nAChR are mediated by His38 and Asp41 from HAEE tetrapeptide site of α4 subunit of the receptor.
(ii) Along with the post-translational modifications of Aβ, hereditary mutations were found in certain patients, some of which lie in the region of the metal-binding domain 1-16. Such mutations affect the toxicity and rate of Aβ oligomerisation in the presence of zinc ions, causing the development of early onset AD. Among them, the Aβ peptide with the "Taiwanese" mutation (D7H-Aβ) has the greatest aggregation ability (Istrate, Kozin et al. 2016). We have investigated the molecular mechanism of zinc-induced oligomerisation of the metal-binding domain of D7H-Aβ(1-16). The critical role of 7 and 13 histidine residues in enhancing the aggregation properties of the peptide D7H-Aβ(1-16) is established by using turbidity measurements, isothermal titration calorimetry and mass-spectrometry. It is shown that the primary binding site of the zinc ion in the D7H-Aβ(1-16) peptide is the 11EVHH14 site, and the E11 and H14 residues of the interacting peptides form a symmetrical zinc-bound intermolecular dimer interface. Then, in this dimer, the E3/H6 and H7/H13 pairs form two more interfaces, through which the formation of D7H-Aβ(1-16) oligomers and aggregates in the presence of zinc ions occurs. Thus, the D7H mutation leads to the emergence of a new mechanism of the zinc-dependent oligomerisation of the metal-binding domain of Aβ(1-16): the role of E11/H14 as primary zinc-bound interface is preserved (as for the zinc-dependent dimer Aβ(1-16)), but the association constant for this site is increased by an order of magnitude, and instead of the H6/H13 interface found for Aβ(1-16) zinc-bound oligomers, two interfaces appear - E3/H6 and H7/H13. This mechanism explains why Aβ(1-16) with the "Taiwanese" mutation, D7H-Aβ(1-16), is the most prone to zinc-induced aggregation in comparison with other Aβ(1-16) isoforms and confirms that 11EVHH14 is a universal target for drugs aimed to suppress zinc-dependent oligomerisation of various Aβ isoforms.

(iii) We have analysed changes in the lifespan of transgenic nematodes *C. elegans* CL2120 (dvis14 [(pCL12) unc-54 :: beta 1-42 + (pCL26) mtl-2 :: GFP]) and *C. elegans* CL2122 (dvis15 [(pPD30.38) unc-54 (vector) + (pCL26) mtl-2 :: GFP]) (obtained from Caenorhaditis Genetics Center) by adding to the culture medium various molecular agents (Aβ, isoD7-Aβ, zinc ions), which are present in amyloid plaques of patients with AD, as well as the tetrapeptide Acetyl-HAEE-NH_2, which is known to be a specific inhibitor of zinc-dependent Aβ oligomerisation and cerebral amyloidogenesis in vivo (Tsvetkov, Cheglakov et al. 2015). It was shown that the simultaneous addition of zinc ions and isoD7-Aβ leads to a significant decrease in the average lifespan of nematodes, which indicates a sharp increase in the integral toxicity of endogenous Aβ aggregates, which are formed, presumably, by a zinc-induced mechanism under the action of seeding centers with the participation of isoD7-Aβ. At the same time, the presence of the tetrapeptide Acetyl-HAEE-NH2 in the nutrient medium completely neutralises the negative effects of the combination of zinc ions and isoD7-Aβ on the lifespan of nematodes. The results obtained indicate the fundamental role of non-covalent complexes between the zinc ion and isoD7-Aβ as a trigger for pathological aggregation of endogenous Aβ molecules. Also, using the tetrapeptide Acetyl-HAEE-NH_2 as an example, it was confirmed that molecular agents that suppress the ability of isoD7-Aβ to participate in zinc-dependent oligomerisation can act as potential drugs that stop the development of cerebral almyloidogenesis in Alzheimer's disease.

Results Unforeseen in the Original Project:

On the basis of our findings on zinc-induced oligomerisation of the metal-binding domain of various Aβ species, we hypothesise that upon phosphorylation of Ser8, isoD7-Aβ loses its ability to form zinc-bound oligomeric seeds. We have found that: (i) *in vitro* isoD7-Aβ with phosphorylated Ser8 (isoD7-pS8-Aβ) is less prone to spontaneous and zinc-induced aggregation in comparison with isoD7-Aβ and intact Aβ as shown by thioflavin T fluorimetry and dynamic light scattering data, and (ii) intravenous injections of isoD7-pS8-Aβ significantly slow down the progression of institutional β-amyloidosis in AβPP/PS1 transgenic mice as shown by the reduction of the congophilic amyloid plaques' number in the hippocampus. The results support the role of the zinc-mediated oligomerisation of Aβ species in the modulation of cerebral β-amyloidosis and demonstrate that isoD7-pS8-Aβ can serve as a potential molecular tool to block the aggregation of endogenous Aβ in AD.

Publications:

Kozin, S.A., Barykin, E.P., Telegin, G.B., Chernov, A.S., Adzhubei, A.A., Radko, S.P., Mitkevich, V.A., Makarov, A.A. Intravenously injected amyloid-β peptide with isomerised Asp7 and phosphorylated Ser8 residues inhibits cerebral β-amyloidosis in AβPP/PS1 transgenic mice model of Alzheimer's Disease. 2018. Front. Neurosci. **12**, 518

TURKEY

Title: Functional and molecular characterization of novel mitotic exit inhibitors
Principal Investigator: Ayse Koca Caydasi, Cell Cycle and Genome Stability Laboratory, Molecular Biology and Genetics Department, College of Sciences, Koç University, Rumelifeneri Yolu, Istanbul, Turkey. Tel: +90-212-3381799, Fax: +90-212-3381205, E-mail: aykoca@ku.edu.tr
ICGEB Contract No.: CRP/18/006
ICGEB Reference No.: CRP/TUR17-04_EC
Abstract: Mitotic exit, the transition from mitosis to G1 phase, is a critical step in the life of a cell and it has to be well regulated. In order for cells to exit mitosis, cyclin-dependent kinase (Cdk) activity has to be down regulated after sister chromatid separation and chromosome segregation. Cdk inactivation relies upon the interplay of mitotic cyclin degradation, Cdk inhibitors and reversal of the Cdk1-Cyclin B driven phosphorylation events that promoted the mitotic state in the first place. A single conserved phosphatase, Cdc14, drives mitotic exit in *Saccharomyces cerevisiae.* In this study we identified the bud cortex protein Bud14 as a novel mitotic exit inhibitor in budding yeast. We further showed that Bud14 together with protein phosphatase 1, Glc7, is a part of the Spindle Position Checkpoint, which halts mitotic exit in response to the failure of spindle positioning along the cell polarity axis. We anticipate that similar mechanisms apply in higher eukaryotes.
Results Obtained:
Among 29 genes identified in a genetic screen that is designed to find mitotic exit inhibitors, one gene, Bud14, was found to be a part of Spindle Position Checkpoint, which halts mitotic exit in response to the failure of spindle positioning along the budding yeast polarity (SPOC) axis. We showed that Bud14 works together with the protein phosphatase 1, Glc7, to promote activity of the SPOC downstream effector Bfa1-Bub2 through dephosphorylation of Bfa1.
Results Unforeseen in the Original Project:
Interestingly, only one gene among many was found to be involved in a known checkpoint. It will be interesting to uncover the roles of remaining genes.
Publications:
Kocakaplan, D., Karaburk, H., Kirdok, I., Erkan, S.N., Dilege, C., Caydasi, A.K. Protein Phosphatase 1 in association with Bud14 inhibits mitotic exit in *Saccharomyces cerevisiae*. 2020. bioRxiv 273946

VIET NAM

Title: Development a simple, low-cost, high sensitivity fluorescent biosensor for hydrogen peroxide (H_2O_2), glucose and cholesterol sensing based on ZnO nanorods decorated metal nanoparticles

Principal Investigator: Hanh Hong Mai, VNU Key Laboratory Multiscale Simulation of Complex Systems, Faculty of Physics, VNU University of Science, 334 Nguyen Trai, Thanh Xuan district, Hanoi, Viet Nam. Tel: +84-967-292460, E-mail: hanhhongmai@hus.edu.vn

ICGEB Contract No.: CRP/18/007
ICGEB Reference No.: CRP/VNM17-03

Abstract: In chemical, biological, clinical, environmental applications the detection of hydrogen peroxide (H_2O_2) is of vital important. It is due to the fact that H_2O_2 can be harmful to biological systems and appears to be involved in the neuropathology of central nervous system diseases. For example, the H_2O_2 level in urine is considered as a potential biomarker for oxidation stress in patients with a malignancy. Recently, diabetes is one of the leading causes of death and disability around the world. When the glucose concentration in human blood is not regulated, life threatening diseases, such as diabetic mellitus and acute diabetes, develop. Cholesterol and its fatty acid esters, on the other hand, are one of the main constituents for the human beings as they are the components of nerve and brain cells; they are precursors of other biological materials, such as bile acid and steroid hormones. High serum cholesterol level is often related to various clinical disorders, such as heart disease, coronary artery disease, arteriosclerosis, hypertension, cerebral thrombosis, etc. In recent years, a new kind of H_2O_2, glucose and cholesterol sensing methodology called fluorescent based methodology has been attracted a lot of attention. Comparing to the conventional electrochemical methods, the fluorescent-based method is a non-destructive testing and do not require the implementation of electrodes. These are the outstanding advantageous of the fluorescence-based methods in designing biosensor devices. Herein, the change in fluorescence of luminescent materials such as nanoparticles or a semiconductor can be used as an indicator of the presence and the concentration of target substances such as H_2O_2, glucose or cholesterol.

In this project, we aim to develop a simple, low-cost, high sensitive fluorescent biosensor for hydrogen peroxide (H_2O_2), glucose and cholesterol sensing. The fluorescent biosensor is based on ZnO nanorods (NRS) decorated with metal nanoparticles (or can be called as nano-heterostructure of ZnO NRs/metal nanoparticles). The working principle of the biosensor is based on the detection of H_2O_2/glucose/cholesterol immobilised directly on ZnO NRs/metal nanoparticles through the photoluminescent quenching of ZnO NRs decorated with metal nanoparticles. The presence of the H_2O_2/glucose/cholesterol will give rise to the corresponding change of photoluminescent signals, which in turn can be used for the detection of glucose and cholesterol concentration in the solution. Due to the presence of metal nanoparticles, the sensitivity and the limit of detection of the sensor will be significantly enhanced compared to the case of bare ZnO nanostructures based fluorescent biosensor.

Objectives:

In this project, we aim to develop a simple, low-cost, high sensitive fluorescent biosensor for hydrogen peroxide (H_2O_2), glucose and cholesterol sensing. Based on this main objective, we clarified into three objectives as follow:

(i) To succeed in synthesising ZnO NRs decorated metal nanoparticles with high density, high vertical alignment, and high crystallinity;

(ii) To succeed in investigating the fluorescent behaviours of the as-synthesised ZnO NRs decorated metal nanoparticles treated with target substances such as H_2O_2, glucose or cholesterol. Investigate the sensitivity, the limit of detection, the selectivity and the response time of the sensor;

(iii) To succeed in clarify the accuracy of the proposed fluorescent sensor when it is treated with real blood sample;

(iv) Upgrading the current free beam Photoluminescence setup for further applications.

Results Obtained:

In this study ZnO NRs/Au NPs were successfully synthesised and implemented for non-enzymatic fluorescent glucose sensing. It was shown that due to the adhesion of Au NPs, the sensitivity was significantly increased in compared with that of the sensor based ZnO NRs. The sensor exhibits a working range of 0.01 mM – 12 mM with a remarkable sensitivity, for example it of (22 ± 2) % mM-1 for glucose sensing, and of (29 ± 2) % mM-1 for H_2O_2 sensing in the range of less than 2 mM. The sensor's sensitivity is at least 7 times higher than other fluorescent sensors. This ultra-high sensitivity enables its application in non-invasive, highly sensitive glucose devices, which can monitor glucose levels in low glucose concentration fluids such as tears, sweat, and saliva. Additionally, good selectivity, high response time are other advantages of the proposed sensor. The significant enhancement in sensitivity is due to surface plasmon resonance effect, while the good selectivity toward other interfering species is probably based on energy level matching of ZnO NRs decorated metal nanoparticles. Most importantly, when treated with human blood serum, the sensor exhibits a high accuracy, which is compatible with that of clinical devices. This ensures the potential application

of ZnO NRs decorated metal nanoparticles for a single use, high sensitivity, high selectivity, non-invasive glucose sensing in clinical measurements.

Results Unforeseen in the Original Project:

The upgraded fluorescent setup can also be used for lasing emission investigation from biological microspheres.

Publications:

Mai, H.H., Janssens, E. Au nanoparticle–decorated ZnO nanorods as fluorescent non-enzymatic glucose sensor. 2020. Microchim. Acta **187**, 577

Mai, H.H., Nguyen, T.T., Gian,g K.M., Do, X.T., Nguyen, T.T., Hoang, H.C., Ta, V.D. Soft Matter. 2020. (in press)